

Ideal MHD stability limits of the PROTO-SPHERA configuration

This article has been downloaded from IOPscience. Please scroll down to see the full text article.

2010 Nucl. Fusion 50 095004

(<http://iopscience.iop.org/0029-5515/50/9/095004>)

View [the table of contents for this issue](#), or go to the [journal homepage](#) for more

Download details:

IP Address: 192.107.52.30

The article was downloaded on 06/09/2010 at 11:02

Please note that [terms and conditions apply](#).

Ideal MHD stability limits of the PROTO-SPHERA configuration

P. Micozzi¹, F. Alladio¹, A. Mancuso¹ and F. Rogier²

¹ Associazione EURATOM-ENEA sulla Fusione, CR Frascati, C.P. 65-00044, Frascati, Rome, Italy

² ONERA-CERT/DTIM/M2SN 2, avenue Edouard Belin-BP 4025-31055, Toulouse Cedex 4, France

E-mail: paolo.micozzi@enea.it

Received 17 November 2009, accepted for publication 14 June 2010

Published 30 July 2010

Online at stacks.iop.org/NF/50/095004

Abstract

The PROTO-SPHERA experiment (under construction in Frascati inside the START vacuum vessel) aims to study the properties of a spherical torus (ST), where a hydrogen force-free screw pinch (SP, with open field lines and fed by electrodes) replaces the central rod of the standard spherical tokamak experiments: PROTO-SPHERA, with a central screw pinch current $I_e = 60$ kA, aims at producing a spherical torus (with closed field lines) of diameter $2R_{\text{sph}} = 70$ cm, and aspect ratio $R/a = A = 1.2\text{--}1.3$, carrying a toroidal current $I_p = 120\text{--}240$ kA. Such a configuration is an evolution of the flux core spheromak (FCS) concept, first proposed by Taylor. The formation mechanism of the configuration will be the one successfully developed by the TS-3 team at the University of Tokyo. The spherical torus toroidal current should be sustained by helicity injection from the screw pinch, therefore some level of resistive instability with toroidal mode numbers $n = 1$ and/or $n = 2$ is requested after the formation and during the sustainment phase; nevertheless, the configuration should be operated such as to maintain it stable from an ideal MHD point of view. The ideal MHD stability limits of PROTO-SPHERA have been analysed by a numerical code able to handle magnetic configurations endowed with both closed and open magnetic field lines. The results of such an analysis are presented in terms of the main parameter, which is the ratio between the currents in the spherical torus and in the central screw pinch, I_p/I_e , and of other relevant parameters of the ST (elongation, aspect ratio, total beta and the toroidal plasma current profile). A comparison with the TS-3 results is also shown.

(Some figures in this article are in colour only in the electronic version)

1. Introduction

A spherical tokamak fusion power plant would have the important advantage of allowing for large toroidal plasma current I_p with a low value of the toroidal magnetic field B_T and therefore for a plasma β ($\beta_{\text{ST}} = 2\mu_0\langle p \rangle_{\text{vol}}/\langle B^2 \rangle_{\text{vol}}$, where p is the plasma kinetic pressure and ST indicates the volume average over the plasma torus) much higher with respect to conventional tokamaks. In the case of spherical tori, for sake of simplicity, the toroidal beta is usually defined in terms of the vacuum toroidal field (which is indicated as B_{T0} , at the reference major radius of the machine R_0) as $\beta_{T0} = 2\mu_0\langle p \rangle_{\text{vol}}/B_{T0}^2$. Indeed values of toroidal beta β_{T0} much larger (up to a factor of 4) than the values obtained in conventional aspect ratio tokamaks (at most $\beta_{T0} \sim 10\%$) have been measured in START [1]: $\beta_{T0} \sim 40\%$, and have been confirmed in later experiments such as MAST: $\beta_{T0} \sim 15\%$ [2] and NSTX: $\beta_{T0} \sim 40\%$ [3]. If, however, the normalized beta value is used, $\beta_N = \beta_{T0}(aB_{T0}/I_p)$ (a being the plasma minor radius), then the values of β_N for spherical tokamaks is higher

(β_N up to 7), but not by any more than a factor of 4, which only reflects the fact that the plasma current is also much enhanced.

A spherical tokamak fusion power plant would unfortunately concentrate most of its engineering difficulties around the toroidal field centre stack, where the magnetic fields and therefore the electromechanical stresses are the highest, and which, due to its slimness, cannot be shielded from neutrons. In the same way, the almost inexistent space allowable for a central solenoid makes it mandatory to also sustain a magnetic fusion configuration of this kind through current drive, which would become particularly demanding (even with respect to conventional tokamak power plants), due to the large toroidal plasma current I_p and to the low value of the toroidal magnetic field B_T .

An intriguing possibility is to substitute the metal centre post current (I_{TF}) with the plasma current of a screw pinch (I_e), driven by dc electrodes. In this way, two problems are potentially solved: first the already mentioned damage of the central conductors disappears and second the helicity injection from the SP to the toroidal plasma closed surfaces should be

able to sustain I_p inside the ST, through cyclic reconnection oscillations of the magnetic configuration, similar to those observed in the FACT [4] and in the SSPX [5] spheromak experiments.

A magnetic configuration of this kind is the so-called flux core spheromak (FCS) concept, first proposed by Taylor [6]. From an experimental point of view, FCS discharges have been obtained both on the TS-3 machine [7] (University of Tokyo) as well as on the SPHEX experiment [8] (UMIST, Manchester). In both cases the characteristics of the obtained toroidal plasma were the ones typical of the classical oblate spheromaks, namely, a safety factor $q < 1$ all over the ST cross-section.

The configuration proposed in the PROTO-SPHERA [9] device (constructed in Frascati inside the START [10] vacuum vessel, $I_e = 60$ kA, ST diameter $2R_{\text{sph}} = 70$ cm, carrying a toroidal current $I_p = 120\text{--}240$ kA) is an evolution of the FCS scheme. The poloidal field (PF) coils of the experiment have been designed in order to obtain a toroidal plasma with high elongation ($\kappa = b/a \approx 2.2\text{--}2.3$) and low aspect ratio ($A \geq 1.2$), allowing for a ST safety factor profile (edge safety factor $q_{95} \approx 3$, safety factor at the magnetic axis $q_0 \geq 1$), quite similar to the one of a metal centre post spherical tokamak. At the same time the PF coils give to the screw pinch plasma, which has a midplane diameter $2\rho_{\text{pinch}(0)} \sim 7$ cm, a disc shape near both electrodes.

Therefore PROTO-SPHERA should be called a ‘flux core spherical tokamak (FCST)’, rather than a FCS. In this way the stability of the configuration should be improved and the helicity current drive may be less disruptive than in the conventional geometry of a FCS, as—for example—the SSPX [5] experiment. Another important characteristic of the PROTO-SPHERA proposal is that it should be possible to decrease the aspect ratio in the course of experiment and to increase the ratio between the toroidal plasma current and the plasma–electrode current, i.e. $I_p/I_e \gg 1$: this is a crucial point in order to obtain plasmas of fusion interest, since the ohmic dissipation in the screw pinch is quite high, due to its low temperature (high parallel transport along the open field lines).

The PROTO-SPHERA formation follows the scheme developed by TS-3 [7]: the initially stable screw pinch is destabilized by increasing the electrode current I_e from 8.5 to 60 kA, the kink instability forms a ST around the SP and this toroidal plasma is compressed by the fast rise in the vertical field [9]. In this sense, the formation can be seen as a tunnelling between two ideal MHD stable states: the initial SP alone and the final SP + ST coupled configuration; it is obvious that some level of resistive instability, even with low toroidal mode numbers ($n = 1$ to 3), must be present during the formation and the sustainment phase, in order to allow for plasma reconnections to inject helicity from SP to ST.

2. A summary of the PROTO-SPHERA equilibria

The method for calculating the PROTO-SPHERA equilibrium configurations, already illustrated in detail in a previous paper [9], is summarized here for the convenience of the reader. In all the cases this paper deals with free-boundary axisymmetric equilibria, calculated in terms of the poloidal flux function,

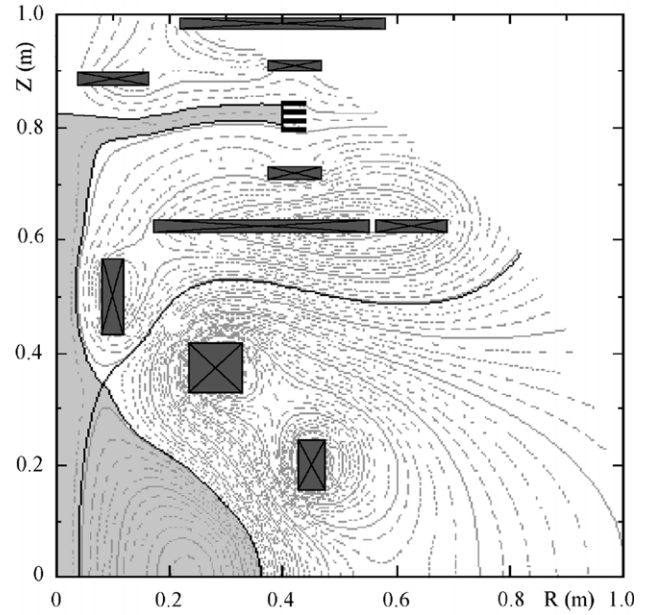


Figure 1. Equilibrium calculation for PROTO-SPHERA: $I_p = 180$ kA, $I_e = 60$ kA, $\beta_p^{\text{ST}} = 0.22$. Only the upper part of the (up/down symmetric) configuration is shown. Contour plot of the poloidal flux ψ . The domains where plasma current density flows are light grey filled. The PF coils are shown in darker grey; the two large PF coils near the equator are the spherical torus compression coils, whereas all the other PF coils act as shaping coils for the plasma disc near the electrodes.

defined inside each magnetic surface as $\psi = 2\pi R A_\varphi$ (where R is the distance from the symmetry axis and A_φ is the azimuthal component of the magnetic vector potential). The plasma–electrode contact surfaces are two (upper and lower) cylindrical ribbons with radius $R_{\text{EL}} = 0.40$ m (see figure 1).

The equilibrium is computed assuming the kinetic plasma pressure $p(\psi)$ and the normalized poloidal plasma current $f(\psi)$, defined in terms of the diamagnetic poloidal current $f(\psi) = \mu_0 I_{\text{dia}}(\psi)/2\pi = RB_\varphi$. The SP (central screw pinch, for $0 < \psi < \psi_X$) is always modelled as a homogeneous force-free plasma that contains two degenerate X-point at $R = 0$ and has no gradient in the kinetic pressure ($\vec{\nabla} p = 0$) or in the relaxation parameter $\langle \mu \rangle = \mu_0 (\vec{J} \cdot \vec{B}/B^2)$ ($\vec{\nabla} \mu = \vec{\nabla} \langle \mu \rangle = 0$), which means $p(\psi) = p_{\text{edge}} = \text{constant}$ and $2\pi f(\psi) = \mu_0 I_e (\psi/\psi_X) = \mu_{\text{SP}} \psi$. The SP–ST interface ($\psi = \psi_X$) is defined by the embedded magnetic separatrix, which contains a standard X-point (with non-vanishing current density on it). Inside the ST ($\psi_X \leq \psi < \psi_{\text{max}}$) the PROTO-SPHERA equilibria are computed, at any time of the formation sequence, assuming either a standard monomial $p(\psi)$ and $f(\psi)$ forms in the Grad–Shafranov equation, namely, $p(\psi) = p_{\text{edge}} + C_p (\psi - \psi_X)^{1.1}$ and $f^2(\psi) = (\mu_0 I_e / 2\pi)^2 + C_f (\psi - \psi_X)^{1.1}$, or the parametric form chosen for the Chandrasekar–Kendall–Furth (CKF) configurations [11], where the region with the largest $\vec{\nabla} p$ in the pressure profile coincides with the region with the largest $\vec{\nabla} \langle \mu \rangle$. In this latter case both gradients are concentrated at the edge of the ST, in the interval $\psi_X \leq \psi \leq \psi_c$, with $\psi_c = \psi_X + h(\psi_{\text{max}} - \psi_X)$; after the ST edge region both the pressure as well as the relaxation parameter remain

constant until the magnetic axis. For $\psi_X \leq \psi \leq \psi_c$:

$$p(\psi) = p_{\text{edge}} \cdot \left\{ 1 + (\Delta p/p_{\text{edge}}) \cdot \left[1 - \cos\left(\frac{\pi(\psi - \psi_X)}{(\psi_c - \psi_X)}\right) \right] \right\},$$

whereas, for $\psi > \psi_c$: $p(\psi) = p_{\text{edge}} \cdot \{1 + (\Delta p/p_{\text{edge}})\}$; correspondingly, for $\psi_X \leq \psi \leq \psi_c$:

$$2\pi f(\psi) = (\mu_{\text{SP}} - \mu_{\text{edge}})\psi_X + \mu_{\text{edge}} \left\{ \psi + \frac{2}{\pi} \left(\frac{\mu_{\text{edge}} - \mu_{\text{axis}}}{\mu_{\text{edge}}} \right) \times (\psi_c - \psi_X) \left[\cos\left(\frac{\pi(\psi - \psi_X)}{2(\psi_c - \psi_X)}\right) - 1 \right] \right\},$$

whereas, for $\psi > \psi_c$:

$$2\pi f(\psi) = (\mu_{\text{SP}} - \mu_{\text{edge}})\psi_X + \mu_{\text{edge}} \left\{ \psi_c - \frac{2}{\pi} \left(\frac{\mu_{\text{edge}} - \mu_{\text{axis}}}{\mu_{\text{edge}}} \right) \times (\psi_c - \psi_X) + \left(\frac{\mu_{\text{axis}}}{\mu_{\text{edge}}} \right) (\psi - \psi_c) \right\}.$$

The h and $(\mu_{\text{edge}} - \mu_{\text{axis}})/\mu_{\text{edge}}$ numbers fix the profile of the relaxation parameter in the ST cross-section, allowing for flatter pressure profiles and stronger shear reversal of the q profiles ($q_0 \gg 1$, $q_{\text{min}} > 1$), with respect to the standard monomial form of $p(\psi)$ and $f(\psi)$; they are kept fixed in this paper: $h = 0.9$ and $(\mu_{\text{edge}} - \mu_{\text{axis}})/\mu_{\text{edge}} = 0.5$. In [9] a larger scan of parameters has been reported.

The total toroidal plasma current flowing inside the ST (I_p) is an input, as well as the poloidal plasma beta:

$$\beta_p^{\text{ST}} = \frac{2}{\mu_0(I_p)^2} \left(\int_{V_{\text{ST}}} p \, dV / V_{\text{ST}} \right) \left(\oint_{C^{\text{ST}}} dl_p \right)^2,$$

which involves an integral over the ST volume V_{ST} for the kinetic pressure and an integral along the contour C^{ST} of the ST cross-section.

The currents in the PF coils (which are also shown in figure 1) are chosen according to the constraints of the PROTO-SPHERA experiment, illustrated in [9]; at any single time of the formation sequence they are kept the same irrespective of the two different ST profile assumptions, monomial or CKF-like; therefore the shape of the plasma slightly changes depending on the assumption. The resulting safety factor profiles are evaluated as the inverse $q(\psi) = 1/\lambda(\psi)$ of the rotational transform

$$\lambda(\psi) = 2\pi \int \left[f(\psi) \oint_{C^{\text{ST}}} \frac{1}{R^2 B_p} dl_p \right],$$

where the integral around the poloidal contour involves the poloidal magnetic field B_p .

A comparison between the safety factor q profiles and the toroidal current density j_ϕ profiles, obtained under the two different assumptions for $p(\psi)$ and $f(\psi)$, is shown in figure 2 for the T6 time. At any single time the poloidal beta β_p^{ST} of the spherical torus has been fixed to the same value under both assumptions for $p(\psi)$ and $f(\psi)$.

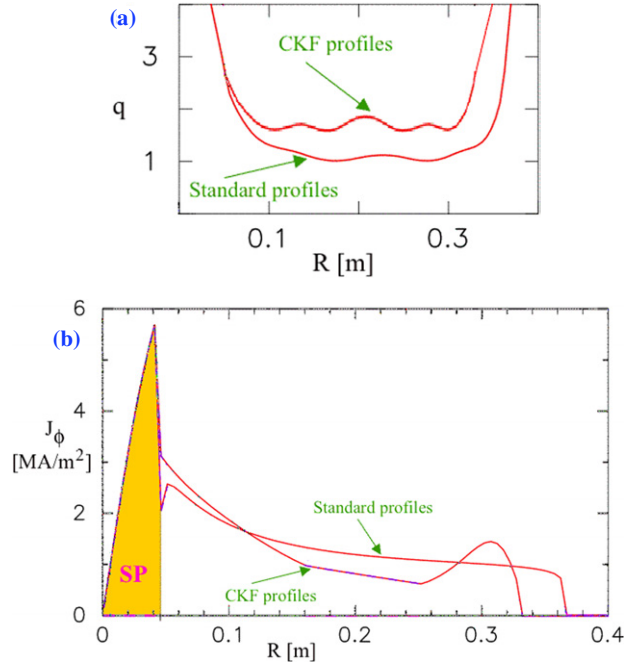


Figure 2. Comparison of time T6 ($I_p = 180$ kA) as computed by using standard and CKF profiles: (a) ST safety factor profile q on the midplane ($Z = 0$), q_{95} is ~ 2.5 in both cases but q_0 rises from 1.1 up to 1.8; (b) toroidal current density profile j_ϕ on the midplane ($Z = 0$), the screw pinch zone is shaded. (Colour online.)

3. Characteristics of the ideal MHD stability code

In the case of PROTO-SPHERA, the coexistence in the same magnetic equilibrium of open and closed field lines, as well as the presence of plasma on the symmetry axis ($R = 0$), introduces peculiar problems in the ideal MHD stability analysis. A free-boundary ideal stability code has been built from scratch on purpose, in order to analyse the ideal MHD operating limits of PROTO-SPHERA. The purpose of this paper is to make a timely presentation of the overall stability results, as the PROTO-SPHERA load assembly is now (2010) built in Frascati and in the next year will start operation. Although the main features of the ideal stability code have been detailed in [12–14], they will be briefly reviewed in this paper for the convenience of the reader.

The perturbed plasma displacement $\vec{\xi}$ is expanded in Boozer [15] magnetic coordinates (ψ_T —radial, i.e. toroidal flux divided by 2π , θ —poloidal, ϕ —toroidal, but different from the geometric azimuth φ). The rotational transform $\lambda(\psi)$ then becomes $\lambda(\psi_T) = -(d\psi/d\psi_T)/2\pi$.

The energy principle is solved through one-dimensional (1D) radial finite elements. It has to be remarked that the standard decomposition [16] of $\vec{\xi}$ in terms of the normal ξ^ψ , binormal η^ψ and parallel μ , namely,

$$\vec{\xi} = \xi^\psi \vec{e}_\psi + \eta^\psi \frac{\vec{B} \wedge \vec{\nabla} \psi_T}{B^2} + \left(\frac{I \eta^\psi}{B^2} - \mu \right) \vec{B}, \quad (1)$$

with

$$\vec{e}_\psi = \frac{\vec{\nabla} \psi_T}{|\vec{\nabla} \psi_T|^2} + \frac{\beta_*}{B^2} \vec{B} - \frac{\gamma_*}{B^2} (\vec{B} \wedge \vec{\nabla} \psi_T) \quad (2)$$

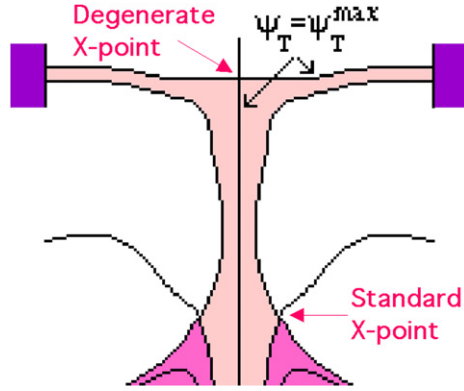


Figure 3. Branching flux surface for the upper part of PROTO-SPHERA. (Colour online.)

(where \vec{e}_ψ is the Boozer covariant radial basis vector, $I(\psi_T) = \mu_0 I_p / 4\pi$ is the normalized toroidal plasma current, $\beta_*(\psi_T, \theta)$ is the non-orthogonality coefficient of the coordinate system [15] and $\gamma_*(\psi_T, \theta)$, is the integrated residual shear [17]) is not appropriate [14] when the plasma extends to the symmetry axis. As a matter of fact on $R = 0$ ($\psi_T = \psi_T^{\max}$, ψ_T being the toroidal flux normalized to 2π), $\vec{\nabla}\psi_T \rightarrow 0$ like $|\vec{\nabla}\psi_T| \propto R$, therefore the regularity condition $\xi^\psi(\psi_T^{\max}) = 0$ must be imposed in the stability solution for the part of the surface $\psi_T = \psi_T^{\max}$ that lies at $R = 0$. However, on the top and bottom of the configuration, after the degenerate X-point ($|B| = 0$), the flux surface with $\psi_T = \psi_T^{\max}$ does not coincide anymore with the symmetry axis (see figure 3), therefore the regularity condition $\xi^\psi(\psi_T^{\max}) = 0$ should not be imposed on the part of the surface $\psi_T = \psi_T^{\max}$ that does not lie at $R = 0$, in any free-boundary ideal MHD stability calculation. The solution of this discrepancy over the boundary condition for different parts of the same flux surface is to change the radial displacement variable to $\xi^\psi = \xi R^N$, with $N \geq 1$; also the binormal displacement variable must be changed to $\eta^\psi = \eta B$, in order to avoid divergences on the degenerate X-point when $|B| = 0$. With these new definitions regularity conditions have no need to be imposed, neither at $R = 0$ nor at the degenerate X-point on the symmetry axis: only when showing the real displacement plots the R^N and B factor have to be properly accounted for in the graphical display.

Further considerations [14] show that the smallest integer exponent which should avoid divergences in the energy principle is $N = 2$. In terms of these new variables (ξ, η, μ) the perturbed displacement becomes

$$\vec{\xi} = \xi R^N \vec{e}_\psi + \eta \frac{\vec{B} \wedge \vec{\nabla}\psi_T}{B} + \left(\frac{I\eta}{B} - \mu \right) \vec{B}. \quad (3)$$

Concerning the magnetic coordinates, particular care has to be taken to match them [12] at the ST-SP interface (see figure 4) and to avoid divergences at the standard and degenerate X-points, in order to guarantee the continuity of the normal contravariant component of the perturbed plasma displacement ξ^ψ between neighbouring radial (ψ_T) mesh points on opposite sides of the embedded magnetic separatrix, a necessary condition in ideal MHD. As illustrated in [12] the field lines are in correspondence at the ST-SP interface

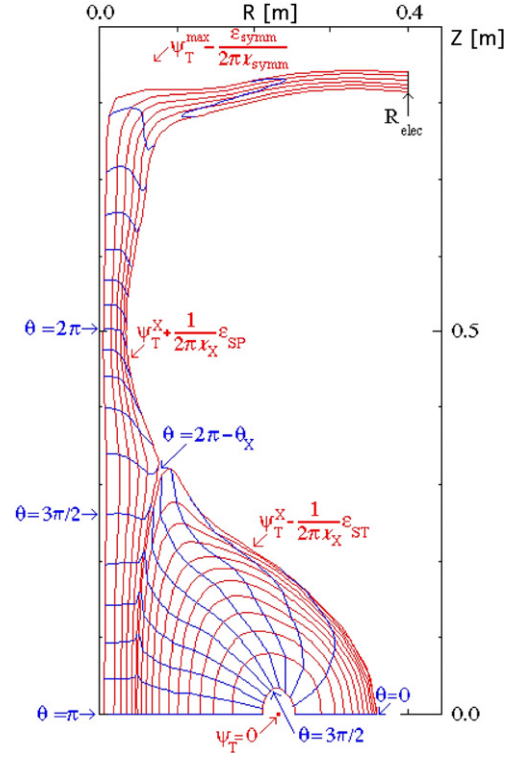


Figure 4. Magnetic coordinates, only the upper part of the (up/down symmetric) configuration is shown. The radial ψ_T coordinate increases from $\psi_T = 0$ on the magnetic axis. The poloidal θ coordinate rotates clockwise from $\theta = 0$ on the outboard of the spherical torus, it is defined by continuity (including the choice $\theta = \pi$ on the inboard) and increases from bottom to top inside the screw pinch. (Colour online.)

along the magnetic separatrix; this implies the continuity of the field line labels $\theta^{\text{ST}} - \int^{\text{ST}}(\psi_T)\phi^{\text{ST}}$ and $\theta^{\text{SP}} - \int^{\text{SP}}(\psi_T)\phi^{\text{SP}}$, between neighbouring radial mesh points on opposite sides of the embedded magnetic separatrix. The correspondence between θ^{SP} and θ^{ST} and ϕ^{SP} and ϕ^{ST} forces the matching condition $\int_{\text{FCS}}^{\text{ST}}(\psi_X + \varepsilon_{\text{ST}}) = \int_{\text{FCS}}^{\text{SP}}(\psi_X - \varepsilon_{\text{SP}})$ for the rotational transform. For the configurations considered here, if the same distance $\varepsilon_{\text{ST}} \approx (1-5) \times 10^{-3} \psi_X$ was used from opposite sides of the magnetic separatrix, the numerically calculated rotational transforms turns out to be only slightly different: $\int_{\text{FCS}}^{\text{SP}}(\psi_X - \varepsilon_{\text{ST}}) \approx \int_{\text{FCS}}^{\text{ST}}(\psi_X + \varepsilon_{\text{ST}})$. This feature makes the matching $\int_{\text{FCS}}^{\text{ST}}(\psi_X + \varepsilon_{\text{ST}}) = \int_{\text{FCS}}^{\text{SP}}(\psi_X - \varepsilon_{\text{SP}}) = \int_X$ a simple recursive calculation in order to obtain the value of ε_{SP} . This condition in particular fixes the poloidal angle θ (see figure 4) in the screw pinch, whose excursion becomes greater than 2π from the lower to the upper electrode (but always less than 4π). Therefore the longest wavelength that can perturb the screw pinch plasma is just the one defined by the common SP-ST interface (from $\theta = 0$ to $\theta = 2\pi$ inside the SP, see the position of $\theta = 2\pi$ marked in figure 4): perturbations able to tear apart the SP from the ST could have a longer wavelength, but they would not be ideal ones. The three components of $\vec{\xi}$ are expanded in a trigonometric Fourier series of modes, assuming up-down symmetry of the equilibrium configuration; each mode is labelled by an index ℓ , which corresponds to a poloidal

number m_ℓ , given the toroidal number n :

$$\begin{aligned}\xi &= \sum_\ell \xi_\ell(\psi_T) \sin(m_\ell \theta - n\phi), \\ \eta &= \sum_\ell \eta_\ell(\psi_T) \cos(m_\ell \theta - n\phi), \\ \mu &= \sum_\ell m_\ell(\psi_T) \cos(m_\ell \theta - n\phi).\end{aligned}$$

For any toroidal number n the normal mode equation, $\delta\vec{W} \cdot |\vec{x}\rangle = \omega^2 \delta\vec{K} \cdot |\vec{x}\rangle$, is solved by a 1D finite-element method, in order to provide the most unstable eigenfunction $|\vec{x}\rangle \equiv (\xi_\ell^j, \eta_\ell^j, \mu_\ell^j)$ (j is the index of the radial mesh) and the corresponding eigenvalue ω^2 of the configuration. Here $\delta\vec{W}$ and $\delta\vec{K}$ are the perturbed potential and kinetic energy matrices: in particular $\delta\vec{W} = \delta\vec{W}_p^i + \delta\vec{W}_p^c + \delta\vec{W}_v$, where $\delta\vec{W}_p^i$ is the incompressible part of the potential energy, $\delta\vec{W}_p^c$ the compressible part and $\delta\vec{W}_v$ the vacuum term.

The simplest boundary condition is the fixed-boundary condition $\xi^\psi(\psi_T^{\text{edge}}) = 0$, which can be directly enforced into the normal mode equation and corresponds to a perfectly conducting shell in contact with the plasma edge. More interesting and more relevant to the analysis of the experimental data is the free-boundary condition, where conducting shells can be placed at a distance from the plasma edge, which is therefore free to move, i.e. $\xi^\psi(\psi_T^{\text{edge}}) \neq 0$.

In this latter case a perturbed vacuum scalar potential Φ is introduced in the vacuum region beyond the equilibrium plasma edge [14]: Φ must be calculated with the appropriate boundary continuity condition at the plasma–vacuum interface $\mu_0 \vec{\nabla} \Phi|_{\psi_T^{\text{edge}}} \cdot d\vec{S}_\psi = -\vec{\nabla} \wedge (\vec{\nabla} \wedge \vec{B})|_{\psi_T^{\text{edge}}} \cdot d\vec{S}_\psi$ and with the appropriate boundary condition on the ideally conducting shells: $\vec{\nabla} \Phi \cdot d\vec{S}_c = 0$. For the calculation of the magnetic energy in the vacuum region surrounding the free-boundary axisymmetric plasma, Green’s function method [18] has been followed.

However, the sophisticated treatment of Green’s function, which is required by the use of a 1D finite-element method (where the elements fill only the contours of the cross-section of the vacuum domain boundaries, i.e. the plasma–vacuum interface and the vacuum–ideal conducting shell boundary) is dispensed in our code [14]: its burden is instead shifted to a 2D finite-element method—where the elements fill the whole cross-section of the vacuum domain (see figure 5); the 2D mesh is able to take into account any axisymmetric shape of stabilizing conductors, which can either surround or not surround the plasma. Furthermore, the perturbed vacuum energy in an open/closed field line configuration like PROTO-SPHERA must be dealt with in an unconventional manner, as stressed in [14]: the vacuum contribution to the potential energy does not only affect the last point of the radial mesh ($\psi_T = \psi_T^{\text{max}} - \varepsilon_{\text{symm}}/2\pi l_{\text{symm}}$, see figure 4), as in a standard tokamak limited by a magnetic separatrix, but also affects the mesh points adjacent to the two sides of the interface between the ST and the SP: $\psi_T = \psi_T^X - \varepsilon_{\text{ST}}/2\pi l_X$ and $\psi_T = \psi_T^X + \varepsilon_{\text{SP}}/2\pi l_X$, see figure 4. On the other hand, no boundary condition for the perturbed displacement has been used on the ribbon surface of the electrodes (see figure 3 and 4),

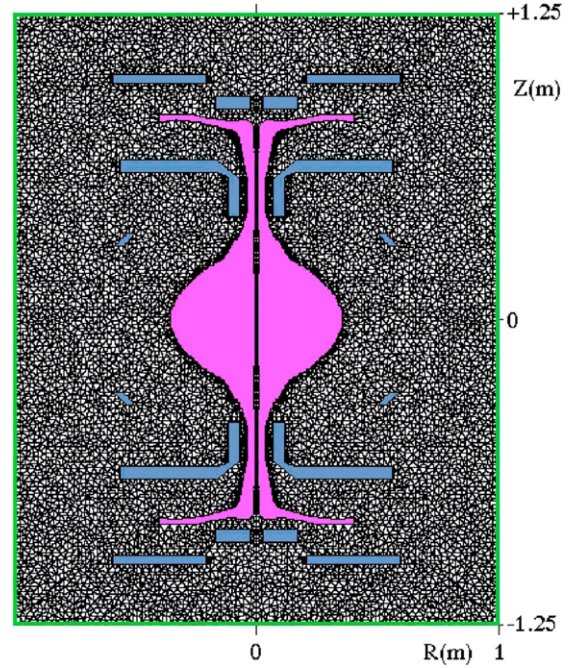


Figure 5. Vacuum finite-element mesh used for PROTO-SPHERA: the plasma is shown as well as the stabilizing conductors, which include the external vacuum vessel and the internal thick casings around some of the plasma disc shaping PF coils. (Colour online.)

which have been built as ‘most irregular’ as possible, in order to maximize the spread of power and current density upon them. The cathode is in reality not a surface, but a large number of tungsten double-spiral filaments; the anode is a ring block of copper, protected on its plasma facing surface by copper–tungsten plates, but is fully carved by a large number of holes through which the hydrogen gas will be injected (hollow gas-puffed anode); therefore the plasma should diffuse as much as possible inside the metal structures of both electrodes and it would be incorrect to presume any kind of line-tying effect.

4. Stability of the PROTO-SPHERA equilibria

The analysis of the PROTO-SPHERA configuration deals with the complete formation sequence of the experiment [9] and investigates the ideal plasma beta ($\beta = 2\mu_0 \langle p \rangle_{\text{vol}} / \langle B^2 \rangle_{\text{vol}}$) limit in the spherical torus, for toroidal mode numbers $n = 1, 2, 3$.

The times considered in this paper—which correspond to the progress of the ST formation—are dubbed, in order of increasing ST toroidal current, as T3 ($I_p = 30$ kA), T4 ($I_p = 60$ kA), T5 ($I_p = 120$ kA), T6 ($I_p = 180$ kA) and TF ($I_p = 240$ kA). In all the cases the longitudinal SP current flowing between the electrodes is kept constant at $I_e = 60$ kA. For the first time T3 ($I_p/I_e = 0.5$), with standard monomial profiles ($I_p = 30$ kA, $A = 1.8$, $\kappa = 2.2$, $q_{95} = 3.4$, $q_0 = 1.2$, $\beta_p^{\text{ST}} = 1.15$, $\beta_N = 10$ and $\beta = 22\%$), the code shows ideal stability for all low toroidal mode numbers $n = 1, 2, 3$ —namely $\omega^2/\omega_A^2 > 0$, ω_A being the Alfvén frequency, $\omega_A^2 = B_0^2/\mu_0 \rho_0 R_0^2$, where B_0 is the magnetic field on the ST axis R_0 and ρ_0 is the mass density assumed constant all over the plasma. The T3 time is also found to be ideally stable when the

equilibrium is computed with the CKF profiles ($I_p = 30$ kA, $A = 1.9$, $\kappa = 2.4$, $q_{95} = 3.3$, $q_0 = 2.1$, $\beta_p^{ST} = 1.15$, $\beta_N = 9.7$ and $\beta = 24\%$).

In a similar way the time T4 ($I_p/I_e = 1$), computed using either the standard monomial profiles ($I_p = 60$ kA, $A = 1.5$, $\kappa = 2.1$, $q_{95} = 2.9$, $q_0 = 1.1$, $\beta_p^{ST} = 0.5$, $\beta_N = 6.9$ and $\beta = 21\%$), or the CKF profiles ($I_p = 60$ kA, $A = 1.6$, $\kappa = 2.4$, $q_{95} = 3.1$, $q_0 = 2.6$, $\beta_p^{ST} = 0.5$, $\beta_N = 6.8$ and $\beta = 26\%$), is found to be ideally stable for low toroidal numbers $n = 1, 2, 3$.

The results change at the time T5 ($I_p/I_e = 2$): using the standard monomial profiles ($I_p = 120$ kA, $A = 1.3$, $\kappa = 2.1$, $q_{95} = 2.8$, $q_0 = 1.0$, $\beta_p^{ST} = 0.3$, $\beta_N = 6.9$ and $\beta = 25\%$), the $n = 1$ toroidal mode number is stable, but the higher toroidal n numbers are unstable ($\omega^2/\omega_A^2 = -1.69 \times 10^{-5}$ for $n = 2$ and $\omega^2/\omega_A^2 = -1.92 \times 10^{-4}$ for $n = 3$). Also using the CKF profiles ($I_p = 120$ kA, $A = 1.4$, $\kappa = 2.5$, $q_{95} = 3.5$, $q_0 = 2.8$, maintaining the poloidal beta at $\beta_p^{ST} = 0.3$, which gives for the CKF profiles a higher plasma beta, $\beta = 33\%$ with $\beta_N = 6.3$) the results remain the same as for the monomial profiles: only the $n = 1$ toroidal mode number is found ideally stable: $\omega^2/\omega_A^2 > 0$ for $n = 1$, whereas the higher toroidal n numbers are unstable: $\omega^2/\omega_A^2 = -2.35 \times 10^{-4}$ for $n = 2$ and $\omega^2/\omega_A^2 = -3.90 \times 10^{-4}$ for $n = 3$. Figure 6(a) shows the perturbed displacement plots in a poloidal cross-section inside the ST and in a horizontal cross-section inside the screw pinch: a global mode is clearly visible both inside the ST as well as inside the SP, but perturbed motions inside the screw pinch are concentrated near the interface with the ST. In order to obtain stability at the time T5, the poloidal beta must be lowered to $\beta_p^{ST} = 0.2$: both the standard monomial profile ($A = 1.4$, $\kappa = 2.2$, $q_{95} = 2.7$, $q_0 = 1.2$, $\beta_N = 4.6$ and $\beta = 16\%$) as well as the CKF profile case ($A = 1.4$, $\kappa = 2.4$, $q_{95} = 2.7$, $q_0 = 1.9$, $\beta_N = 4.4$ and $\beta = 18\%$) are completely stabilized. Figures 6(b) and (c) show the perturbed displacement plots for $n = 2$ and $n = 3$ (standard profiles): only damped ($\omega^2/\omega_A^2 > 0$) motions appear, respectively, around the $q = 3/2$ resonant surface inside the ST and around the $q = 2$ surface inside the SP, and can be interpreted as stabilized localized interchange modes.

At the later time T6 ($I_p/I_e = 3$), using the standard monomial profiles ($I_p = 180$ kA, $A = 1.25$, $\kappa = 2.2$, $q_{95} = 2.6$, $q_0 = 0.96$, $\beta_p^{ST} = 0.225$, $\beta_N = 6.7$ and $\beta = 25\%$), the mode with toroidal number $n = 1$ is stable, whereas $n = 2$ and $n = 3$ are unstable; instead, using the CKF profiles ($I_p = 180$ kA, $A = 1.29$, $\kappa = 2.5$, $q_{95} = 3.2$, $q_0 = 2.3$, $\beta_p^{ST} = 0.225$, $\beta_N = 6.1$ and $\beta = 33\%$), all low toroidal mode numbers become ideally unstable: $\omega^2/\omega_A^2 = -6.84 \times 10^{-4}$ for $n = 1$, $\omega^2/\omega_A^2 = -4.62 \times 10^{-3}$ for $n = 2$ and $\omega^2/\omega_A^2 = -3.40 \times 10^{-3}$ for $n = 3$.

This result shows that at high beta (and the CKF equilibrium profile has, with the same β_p^{ST} , a higher plasma beta than the monomial equilibrium profile) it is necessary to push the current ratio up to $I_p/I_e = 3$ in order to drive a tilting ideal instability, i.e. a destabilization of the toroidal mode number $n = 1$, which tilts the spherical torus, while displacing as a kink the screw pinch: therefore it is the SP that drives the instability of the coupled configuration. The reason for the $n = 2$ and $n = 3$ instabilities is quite different: if the ideal stability is computed for the spherical torus alone

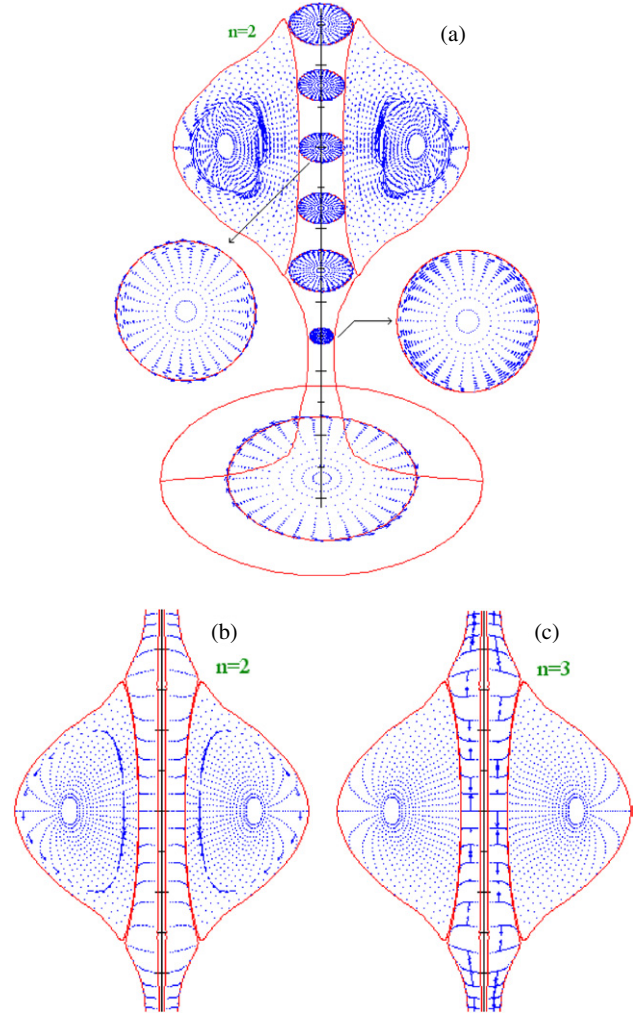


Figure 6. Arrow plots of perturbed displacement at T5 time, with monomial profiles: (a) unstable to $n = 2$ mode at higher $\beta = 25\%$; (b) stable to $n = 2$ mode and (c) stable to $n = 3$ at lower $\beta = 16\%$ (damped— $\omega^2/\omega_A^2 > 0$ —localized motions). (Colour online.)

(i.e. forgetting the presence of the SP discharge) it turns out that the ST is unstable (even if fixed-boundary conditions are applied for the perturbations at its edge) for the toroidal mode numbers $n = 2$ and $n = 3$, while it remains stable for $n = 1$; therefore, whereas for $n = 1$ the SP destabilizes the ST, for higher mode numbers the screw pinch instead acts as a stabilizer for the spherical torus. The influence of the vacuum term can be estimated by removing the thick metal casings, indicated in figure 5 around PF coils that shape the plasma discs, and which by the way do not surround completely the plasma, leaving therefore only the vacuum vessel as a very remote stabilizing shell; in such a case the strength of the $n = 1$ mode instability (CKF profiles, $\beta_p^{ST} = 0.225$ and $\beta = 33\%$) increases only slightly, from $\omega^2/\omega_A^2 = -6.84 \times 10^{-4}$ to $\omega^2/\omega_A^2 = -7.00 \times 10^{-4}$. Therefore the thick metal casings around the plasma disc PF shaping coils have only a marginal influence upon the ideal MHD stability limit; they have indeed been introduced in the experiment for a different reason: to make the equilibrium compatible with the position of the electrodes at all times. It is sufficient to decrease the poloidal beta down to $\beta_p^{ST} = 0.15$ in order to stabilize, at the time T6,

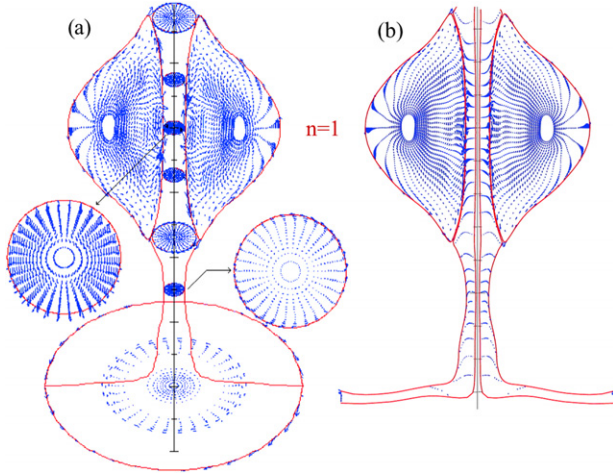


Figure 7. Final (sustainment) time TF with high $\beta = 23\%$ (CKF profiles), unstable to an $n = 1$ tilting mode: the arrows plot shows the perturbed displacement; (a) horizontal section displayed through the screw pinch, (b) vertical section displayed through the screw pinch. (Colour online.)

both the standard monomial profile ($I_p = 180$ kA, $A = 1.29$, $\kappa = 2.2$, $q_{95} = 2.5$, $q_0 = 1.12$, $\beta_N = 4.7$ and $\beta = 15\%$) as well as the CKF profile case ($I_p = 180$ kA, $A = 1.32$, $\kappa = 2.5$, $q_{95} = 2.5$, $q_0 = 1.83$, $\beta_N = 4.3$ and $\beta = 19\%$).

At the ‘flat-top sustainment’ time TF (where the currents ratio increases up to $I_p/I_e = 4$), the ideal MHD behaviour is just the same as at the previous time T6. The standard monomial profile ($I_p = 240$ kA, $A = 1.22$, $\kappa = 2.2$, $q_{95} = 2.65$, $q_0 = 1.04$, $\beta_p^{ST} = 0.15$, $\beta_N = 5.5$ and $\beta = 19\%$) gives stability: $\omega^2/\omega_A^2 > 0$ for $n = 1$, and instability: $\omega^2/\omega_A^2 = -1.61 \times 10^{-4}$ for $n = 2$ and $\omega^2/\omega_A^2 = -9.82 \times 10^{-5}$ for $n = 3$. Similarly the CKF profile ($I_p = 240$ kA, $A = 1.24$, $\kappa = 2.4$, $q_{95} = 2.89$, $q_0 = 1.82$, with the same $\beta_p^{ST} = 0.15$ but with the higher plasma beta $\beta = 23\%$ and $\beta_N = 5.1$) makes the low toroidal mode numbers $n = 1$ and $n = 2$ ideally unstable at the sustainment time TF: $\omega^2/\omega_A^2 = -7.48 \times 10^{-3}$ for $n = 1$, $\omega^2/\omega_A^2 = -1.47 \times 10^{-3}$ for $n = 2$, whereas $\omega^2/\omega_A^2 > 0$ for $n = 3$, due to the stabilizing effect of the reversed shear profile upon the $n > 1$ mode numbers. Figure 7 shows the perturbed displacement plots in a poloidal cross-section inside the ST and in a horizontal cross-section inside the screw pinch (figure 7(a)) as well as in a vertical cross-section (figure 7(b)): a global mode is clearly visible both inside the ST as well as inside the SP, but perturbed motions inside the screw pinch are concentrated near the interface with the ST. Again the ideal stability, computed for the spherical torus alone (i.e. forgetting the presence of the SP discharge) yields a ST unstable (even if fixed-boundary conditions are applied for the perturbations at its edge) for the toroidal mode number $n = 2$, while it remains stable for $n = 1$, confirming that it is the SP that drives the tilting instability of the coupled configuration.

In order to stabilize the sustainment time TF, the poloidal beta must be further lowered to the value $\beta_p^{ST} = 0.12$ for the standard monomial profile ($I_p = 240$ kA, $A = 1.24$, $\kappa = 2.3$, $q_{95} = 2.55$, $q_0 = 1.13$, $\beta_N = 4.4$ and $\beta = 16\%$); the CKF profile needs a slightly deeper lowering of the poloidal beta ($I_p = 240$ kA, $A = 1.26$, $\kappa = 2.4$, $q_{95} = 2.55$, $q_0 = 1.64$,

$\beta_p^{ST} = 0.10$, $\beta_N = 3.5$ and $\beta = 14\%$) to obtain stability, confirming that the ST equilibrium obtained with the CKF profiles makes the coupled configuration more unstable to the $n = 1$ tilt mode.

5. Effect of the configuration geometry and comparison with TS-3 experiment

The ST elongation κ seems to have an important influence on the kink stability of the SP: figure 8 shows that if the PROTO-SPHERA machine ($\kappa = 2.3$) were modified in order to obtain larger elongations ($\kappa = 3$) of the spherical torus, a higher ratio between the ST toroidal current and the SP longitudinal current could be obtained, up to $I_p/I_e \sim 5.5$ at $\beta = 14\%$, without destabilizing the $n = 1$ tilting mode.

The case with larger elongation ($\kappa = 3$) raises the question of the vertical ($n = 0$) stability: indeed, the PROTO-SPHERA machine was conservatively designed to produce ST plasmas with $\kappa \approx 2$. The axisymmetric stability is not analysed in detail in this paper: further improvements of the stability code are needed to correctly assess it; in particular the decomposition of ξ has to be slightly changed with respect to the form reported in equation (3), in order to deal properly with the eigenfunctions near the standard X-points. Nevertheless, a preliminary computation indicates that even the $\kappa = 3$ equilibrium is vertically stable. This fact is not surprising, due to the very low self-inductance of the ST ($l_i \approx 0.2$) and to the straight shape of the vacuum field provided by the PF coils (see figure 8(c)).

In order to assess the stability code, and to further investigate the dependence of the FCS/FCST configuration upon the geometrical details of the plasma shaping, a comparison with the TS-3 FCS experiment [7] has been undertaken. Because of the very limited number of PF coils (two ‘fixed current’ Helmholtz coils outside the vacuum vessel and two compression coils inside), the TS-3 device could not produce a singular X-point on the symmetry axis and neither had plasma discs inside separate electrode chambers, but the central plasma column was simply a screw pinch fed by standard cylindrical electrodes. In the TS-3 experiment the current between the electrodes was pushed up along with the current in the compression coils; the case reported in [7] has been modelled choosing the currents in the compression coils (which were not specified in the TS-3 publication) in order to fit the measured plasma shape at $I_e = 40$ kA, $I_p = 50$ kA (both measured, $I_p/I_e \approx 1$) and $\beta = 13\%$ (estimated from density and temperature measurements): the code yields $\omega^2/\omega_A^2 > 0$ for the $n = 1$ toroidal mode (see figure 9(a)), which is a highly damped motion around the $q_{ST} = 1$ resonance inside the ST as well as around the $q_{SP} = 1$ inside the SP (note that q_{SP} is defined along the symmetry axis—poloidal turns/toroidal turns of a field line—and is therefore reversed with respect to q_{ST} defined along the ST magnetic axis—toroidal turns/poloidal turns of a field line).

On the other hand, if in the simulation the TS-3 toroidal current is pushed up to $I_p = 100$ kA along with the current in the compression coils, still with $I_e = 40$ kA ($I_p/I_e \approx 2$) at $\beta = 13\%$, the code finds a strong $n = 1$ ideal instability with $\omega^2/\omega_A^2 = -1.05$ broadly diffused and not far from the $q_{SP} = 1$ safety factor inside the SP (q_{SP} is by the way increased by the

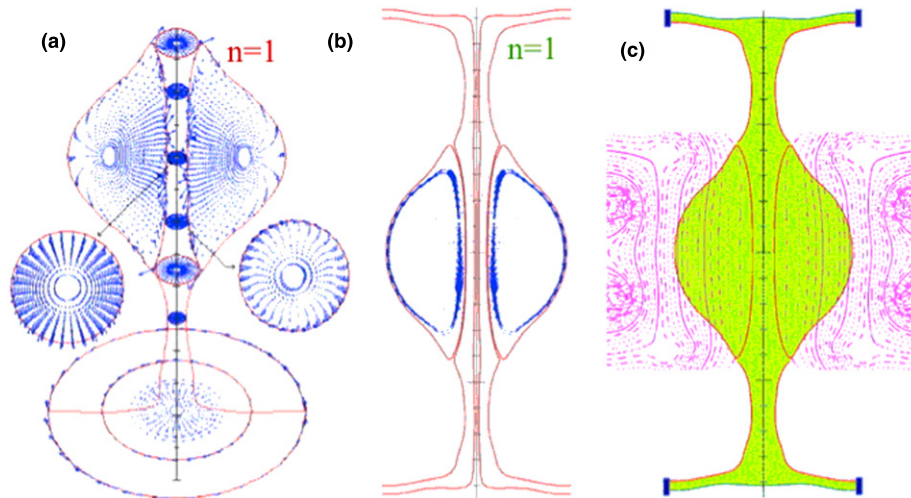


Figure 8. Arrows plot of: (a) the unstable $n = 1$ tilting mode that appears if the ST current of PROTO-SPHERA ($\kappa = 2.3$, $\beta = 14\%$) is pushed up to $I_p/I_e = 5$; (b) if instead the machine elongation could be increased ($\kappa = 3$, $\beta = 14\%$) the $n = 1$ mode would be stabilized (damped localized motions) even if the toroidal current were pushed to the larger values such as $I_p/I_e = 5.5$; (c) flux function of the vacuum field for the PROTO-SPHERA equilibrium with $\kappa = 3$, superimposed to the plasma shape. (Colour online.)

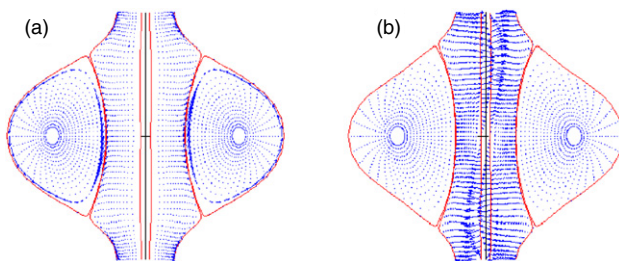


Figure 9. Arrows plot of the perturbed displacement for: (a) stable $n = 1$ damped motion in TS-3 with $I_p = 50$ kA, $I_e = 40$ kA; (b) unstable $n = 1$ mode in TS-3 with $I_p = 100$ kA, $I_e = 40$ kA. (Colour online.)

larger current in the ST, see figure 9(b)), a normalized growth rate almost an order of magnitude larger than the worst found for PROTO-SPHERA in section 4.

As the current flowing in the Helmholtz coils was kept fixed in the actual experiment, the two simulated equilibria of TS-3 shown in figure 9 have a different compression and a slightly different plasma shape (the equilibrium calculated at higher current was of course never obtained in the experiment, as the onset of an ideal instability just makes the plasma vanish on the Alfvén time-scale). The results of the simulation confirm the experimental result that the TS-3 FCS could not achieve a toroidal ST current much higher than $I_p = 50$ kA and that its ST was limited to an aspect ratio not lower than $A = 1.6$: presumably the onset of an ideal MHD instability just led to the disappearance of the plasma.

The value of the safety factor profile inside the spherical torus and the screw pinch of TS-3 flux-core experiment was one of the main reasons for these limitations. However, the presence of plasma discs inside separate electrode chambers play a relevant role in the case of the PROTO-SPHERA configuration: if the screw pinch of the stable T5 time of PROTO-SPHERA ($I_p/I_e = 2$, $\beta = 16\%$) is ‘artificially cut’ in order to eliminate the singular X-points near the electrodes (see figure 10), then the calculated equilibrium becomes ideally

unstable as soon as the disc-shaped plasmas disappear along with the singular X-points: the ideal growth rate reaches $\omega^2/\omega_A^2 = -0.17$ for $n = 1$, not far from the ideal growth rate estimated for TS-3, although the perturbed displacement is stronger near both sides of the ST–SP interface.

The relevance of the plasma discs in the stabilization of PROTO-SPHERA can be understood by the following considerations: at low ratio I_p/I_e and at low β_{ST} the dipole moment of the PF coils near the plasma discs, which provide the correct plasma shape in front of the electrodes, is aligned with the dipole moment of the spherical torus and has therefore a stabilizing effect which dominates over the opposite (tilt destabilizing) dipole moment of the compression PF coils. Instead at high β_{ST} the ST tilt instability is destabilized by an increased opposite dipole moment of the compression PF coils; similarly when the ratio I_p/I_e is increased the SP becomes kink unstable, as it becomes too thin ($\rho_{\text{Pinch}(0)}/R_{\text{sph}} \leq 0.1$) on its midplane, and therefore causes the tilt of the ST.

6. Conclusions

The ideal MHD stability behaviour of PROTO-SPHERA shows large differences with respect to the stability of spherical tokamaks [19]. The presence of two neighbouring plasmas makes it mainly dependent upon the ratio between the toroidal plasma current and the (plasma–electrode) screw pinch current, i.e. I_p/I_e . On the other hand, as the screw pinch current is assumed as force-free, the only remaining beta is the one of the spherical torus: in PROTO-SPHERA the plasma beta limit goes from 21–26% for ST/SP currents ratio in the range $I_p/I_e \leq 1$ down to 14–16% for $I_p/I_e = 4$ (the range of variation—for the same ratio I_p/I_e —depends upon the profiles inside the ST). The behaviour in terms of the limit of β_p^{ST} as a function of I_p/I_e is much steeper and is shown in figure 11.

In order to compare PROTO-SPHERA with a conventional spherical tokamak with central rod, one can use the vacuum toroidal beta β_{T0} ($\beta_{T0} = 2\mu_0 \langle p \rangle_{\text{vol}} / B_{T0}^2$, where for the coupled ST + SP PROTO-SPHERA configuration B_{T0} means

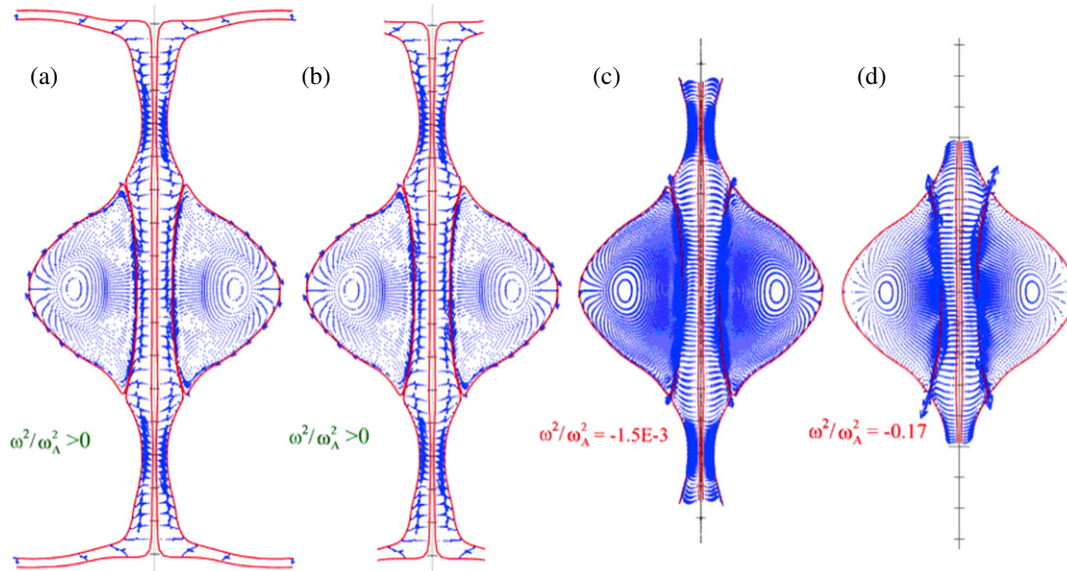


Figure 10. PROTO-SPHERA at time T5 with $I_p = 120$ kA, $I_e = 60$ kA. Arrows plot of the perturbed displacement when the extension of the screw pinch plasma is progressively cut: (a) and (b) stable $n = 1$ damped motion; (c) and (d) unstable $n = 1$ mode (Colour online.)

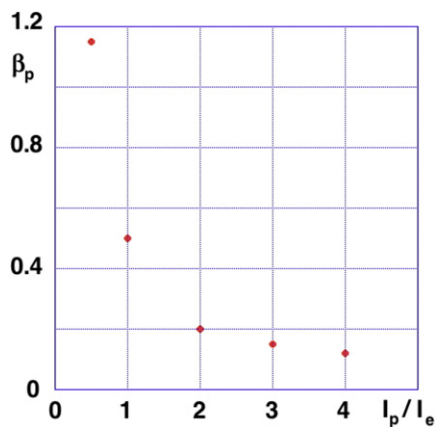


Figure 11. Behaviour of β_p^{ST} as a function of the currents ratio I_p/I_e . (Colour online.)

the toroidal field generated by the longitudinal current I_e on the geometric axis of the ST); with this somewhat artificial definition, the PROTO-SPHERA beta limit would go from $\beta_{T0} = 28\text{--}29\%$ for $I_p/I_e = 0.5$ to $\beta_{T0} = 72\text{--}84\%$ for $I_p/I_e = 4$.

The spherical torus dominates the instabilities up to $I_p/I_e \approx 3$, with $n = 2$ and $n = 3$ toroidal mode numbers: if the ideal stability is computed for the spherical torus alone (i.e. forgetting the presence of the SP discharge), it turns out that the ST is unstable (even if fixed-boundary conditions are applied for the perturbations at its edge) for the toroidal mode numbers $n = 2$ and $n = 3$, while it remains stable for $n = 1$. Therefore, up to $I_p/I_e \approx 3$, the screw pinch instead acts as a stabilizer for the spherical torus: at low ratio I_p/I_e and at low β_{ST} the dipole moment of the PF coils near the plasma discs, which provide the correct plasma shape in front of the electrodes, is aligned with the dipole moment of the spherical torus and has therefore a stabilizing effect which dominates over the opposite (tilt destabilizing) dipole moment of the compression PF coils. The comparison with

the TS-3 experimental results suggests that the disc-shaped screw pinch plasma near both electrodes should be paramount for improving the ideal stability of the PROTO-SPHERA configuration.

Beyond this level of currents ratio, the dominant instability is the kink of the SP that gives rise to the ST tilt motion: at high β_{ST} the ST tilt instability is destabilized by an increased opposite dipole moment of the compression PF coils; similarly when the ratio I_p/I_e is increased the SP becomes kink unstable, as it becomes too thin ($\rho_{\text{Pinch}(0)}/R_{\text{sph}} \leq 0.1$) on its midplane, and therefore causes the tilt of the ST.

Due to the dominant role of the disc-shaped screw pinch plasma near both electrodes, the ideal MHD stability of PROTO-SPHERA is rather insensitive to the internal ST profiles: therefore the configuration should be quite robust from the ideal point of view. On the other hand, the behaviour with respect to the resistive instabilities remains as the main experimental point to be investigated by the PROTO-SPHERA project. As a final remark, it has to be noted that increasing the spherical torus elongation κ could lead to a further increase in the ratio between the toroidal plasma current and the (plasma-electrode) screw pinch current, beyond the limit $I_p/I_e \sim 4$, that has been illustrated in this paper and has been in the design of PROTO-SPHERA.

Euratom © 2010.

References

- [1] Robinson D.C. 1999 *Plasma Phys. Control. Fusion* **41** A143
- [2] Lloyd B. *et al* 2004 *Plasma Phys. Control. Fusion* **46** B477
- [3] Sontag A.C. *et al* 2007 *Nucl. Fusion* **47** 1005
- [4] Nagata M. *et al* 1993 *Phys. Rev. Lett.* **71** 4342
- [5] Stallard B.W. 2003 *Phys. Plasmas* **10** 2912
- [6] Taylor J.B. and Turner M.F. 1989 *Nucl. Fusion* **29** 219
- [7] Amemiya N. *et al* 1993 *J. Phys. Soc. Japan* **63** 1552
- [8] Brennan D. *et al* 1999 *Phys. Plasmas* **6** 4248
- [9] Alladio F. *et al* 2006 *Nucl. Fusion* **46** S613
- [10] Sykes A. *et al* 1992 *Nucl. Fusion* **32** 694

- [11] Rogier F. *et al* 2003 Simply connected high-B magnetic configurations *11th Int. Congress on Plasma Physics: ICPP 2002 American Institute of Physics* vol 669 p 557 <http://scitation.aip.org/dbt/dbt.jsp?KEY=APCPCS&Volume=669&Issue=1> and <http://scitation.aip.org/getabs/servlet/GetabsServlet?prog=normal&id=APCPCS000669000001000557000001&istype=cvips&gifs=yes&ref=no>
- [12] Alladio F. *et al* 2005 *Phys. Plasmas* **12** 112502
- [13] Alladio F. *et al* 2006 *Phys. Plasmas* **13** 082505
- [14] Alladio F. *et al* 2007 *Phys. Plasmas* **14** 082508
- [15] Boozer A.H. 1981 *Phys. Fluids* **24** 1999
- [16] Cooper W.A. 1992 *Plasma Phys. Control. Fusion* **34** 1011
- [17] Pletzer A. *et al* 1994 *J. Comput. Phys.* **115** 530
- [18] Gruber R. *et al* 1981 *Comput. Phys. Commun.* **21** 323
- [19] Sabbagh S. *et al* 2004 *Nucl. Fusion* **44** 560